Probing ∼L_* Lyman-break galaxies at $z \approx 7$ in GOODS-South with WFC3 on *Hubble Space Telescope*

Stephen M. Wilkins,[1]★ Andrew J. Bunker,[1] Richard S. Ellis,[2] Daniel Stark,[3] Elizabeth R. Stanway,[4] Kuenley Chiu,[2] Silvio Lorenzoni[1] and Matt J. Jarvis[5]

[1]*University of Oxford, Department of Physics, Denys Wilkinson Building, Keble Road, Oxford OX1 3RH*
[2]*California Institute of Technology, Astrophysics Department, Mail Stop 169-327, Pasadena, CA 91109, USA*
[3]*University of Cambridge, Institute of Astrophysics, Madingley Road, Cambridge CB3 0HA*
[4]*H H Wills Physics Laboratory, Tyndall Avenue, Bristol BS8 1TL*
[5]*Centre for Astrophysics, Science and Technology Research Institute, University of Hertfordshire, Hatfield, Herts AL10 9AB*

ABSTRACT

We analyse recently acquired near-infrared *Hubble Space Telescope* imaging of the Great Observatories Origins Deep Survey (GOODS)-South field to search for star-forming galaxies at $z \approx 7.0$. By comparing Wide Field Camera 3 (WFC3) 0.98 μm Y-band images with Advanced Camera for Surveys (ACS) z-band (0.85 μm) images, we identify objects with colours consistent with Lyman-break galaxies at $z \simeq 6.4$–7.4. This new data cover an area five times larger than that previously reported in the WFC3 imaging of the *Hubble Ultra Deep Field* and affords a valuable constraint on the bright end of the luminosity function. Using additional imaging of the region in the ACS B, V and i bands from GOODS v2.0 and the WFC3 J band, we attempt to remove any low-redshift interlopers. Our selection criteria yields six candidates brighter than $Y_{AB} = 27.0$, of which all except one are detected in the ACS z-band imaging and are thus unlikely to be transients. Assuming all six candidates are at $z \approx 7$, this implies a surface density of objects brighter than $Y_{AB} = 27.0$ of 0.30 ± 0.12 arcmin^{-2}, a value significantly smaller than the prediction from $z \approx 6$ luminosity function. This suggests continued evolution of the bright end of the luminosity function between $z = 6$ and 7, with number densities lower at higher redshift.

Key words: galaxies: evolution – galaxies: formation – galaxies: high-redshift – galaxies: starburst – ultraviolet: galaxies.

1 INTRODUCTION

In recent years, our understanding of the high-redshift galaxy population has rapidly expanded with the discovery of star-forming galaxies within the first billion years ($z > 5$), through the Lyman-break technique using broad-band imaging (e.g. Stanway, Bunker & McMahon 2003; Dickinson et al. 2004) and searches for Lyman α emission with narrow-band filters (e.g. Ouchi et al. 2008; Ota et al. 2008), and most recently gamma-ray bursts (e.g. Salvaterra et al. 2009; Tanvir et al. 2009). At $z \sim 6$, the brightest ($z < 26.5$) Lyman-break 'i-band dropout' galaxies have been confirmed spectroscopically (e.g. Bunker et al. 2003; Stanway et al. 2004a,b; Dow-Hygelund et al. 2007; Vanzella et al. 2009) through their Lyman α emission, confirming the validity of this photometric redshift selection.

In recent weeks, the installation of the new Wide Field Camera 3 (WFC3) on the *Hubble Space Telescope* (*HST*), which has an

infrared (IR) channel with a large field of view, has enabled the Lyman-break technique to be pushed to $z \sim 7$–10, revealing for the first time significant numbers of galaxy candidates close to the reionization epoch (Bouwens et al. 2009; Bunker et al. 2009; Oesch et al. 2009; Yan et al. 2009; McLure et al. 2010). However, the first data to be released were the extremely deep single pointing on the *Hubble Ultra Deep Field* (HUDF; $\approx$4 arcmin^2), reaching objects as faint at mag$_{AB} = 28.5$ (6 σ) in Y, J and H bands. To probe the rare galaxies at the bright end of the luminosity function (LF) at $z \sim 7$–8 requires a larger field of view. There have been some shallower wider area searches using ground-based observations (e.g. Castellano et al. 2009; Ouchi et al. 2009; Hickey et al. 2010), but the depths probed are typically $Y_{AB} < 26$ (equivalent to $L_{UV} > 2 L^*$) and the numbers of robust candidates are small. Increasing the number of $z \approx 7$ candidates over a wide range of magnitudes is critical to exploring the shape of the LF. This is particularly important as there is strong evidence for evolution of LF, with suggestions that at high redshift there is a larger relative contribution to the stellar mass and ultraviolet (UV) luminosity density from sub-L_* systems. At $z \sim 7$, we are close to the epoch of reionization, and an open

★E-mail: stephen.wilkins@astro.ox.ac.uk (SMW)

question is the mechanism by which reionization is achieved; if we are to address the contribution of the UV from star-forming galaxies, then quantifying the LF is vital (along with the escape fraction of ionizing photons from galaxies and the hardness of the UV spectral slope).
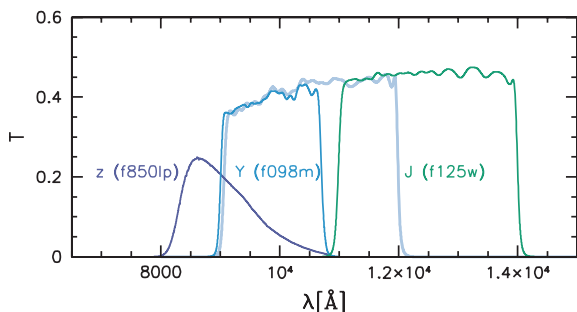
In this paper, we present first results from *HST*/WFC3 imaging of some of the GOODS-South field, covering an area five times that of the WFC3 images of the HUDF and reaching $Y_{AB} = 27.0$ (6σ), probing luminosities around $L_{UV\,z\sim6}^*$. In conjunction with the GOODS v2.0 Advanced Camera for Surveys (ACS) images with B, V, i, z bands (Giavalisco et al. 2004), we search for objects which are much brighter in the Y-band WFC3 filter at 1 μm than the z-band 0.9 μm and are undetected at shorter wavelength. These 'z-drops' are candidate $z \sim 7$ Lyman-break galaxies, and the greater area of this new data set (compared with the HUDF WFC3 images) means that we are likely to find brighter objects more amenable to future spectroscopic confirmation.

The structure of this paper is as follows. In Section 2, the imaging data and the construction of catalogues are described. In Section 3, we describe our candidate selection and discuss the observed surface density of $z \approx 7$ galaxies, comparing with the expected number from a range of LFs. Our conclusions are presented in Section 4. Throughout, we adopt the standard 'concordance' cosmology of $\Omega_M = 0.3$, $\Omega_\Lambda = 0.7$ and use $h_{70} = H_0/70\,\mathrm{km\,s^{-1}\,Mpc^{-1}}$. All magnitudes are on the *AB* system (Oke & Gunn 1983).

2 *HST* OBSERVATIONS AND DATA REDUCTION

We use the *HST* images of GOODS-South obtained with WFC3 under the Early Release Science programme (ERS) GO/DD 11359 (P.I. R. O'Connell). This will ultimately cover 10 pointings with the IR channel within the GOODS-South field, along with UV images of the same area. We focus here on the first six WFC3 pointings to be released (data taken over the period 2009 September 17–27 UT). The observations were split into visits, and each pointing was imaged for two orbits in each filter during a single visit.

Each pointing was imaged in three filters (F098M 'Y band', F125W 'J band' and F160W 'H band'; Fig. 1), and each filter observation comprised two orbits (taken within the same *HST* visit) which were split into three exposures. The near-IR channel of WFC3 has a 1014×1014 Teledyne HgCdTe detector which can be read non-destructively. Each exposure involved a 'MULTIACCUM' sequence of non-destructive reads (the SPARS100 pattern was used, spacing reads by $\approx 100\,\mathrm{s}$), enabling cosmic ray rejection through 'sampling up the ramp'. The exposures comprised nine or 10 non-

destructive readouts, totalling 803–903 s. The IRAF.STSDAS pipeline CALWFC3 was used to calculate the count rate and reject cosmic rays through gradient fitting, as well as subtracting the zeroth read and flat-fielding. From each individual exposure in each filter, we subtracted the median stack of the 36 exposures in the same filter (six per pointing and six pointings), with bright objects excluded from the median using object masks created by the XDIMSUM package. This subtracted out hot pixels and eliminated quadrant pedestal offset effects, as well as correcting for scattered light. We used MULTIDRIZZLE (Koekemoer et al. 2002) to combine the six exposures per filter in each pointing, taking account of the geometric distortions and mapping on to an output pixel size of 0.06 arcsec from an original 0.13 arcsec pix^{-1}. This was the same scale as we used in our analysis of the HUDF WFC3 images (Bunker et al. 2009) and corresponds to a 2×2 block averaging of the GOODS v2.0 ACS drizzled images. The six exposures per pointing were dithered by 10 arcsec, so that bad pixels did not overlap and to facilitate subtraction of any residual background (see above). We found that it was necessary to introduce small corrections to the pointing information in the header to accurately align the exposures in MULTIDRIZZLE (and prevent real objects being rejected by the algorithm). There was a slight discrepancy between the position angle information in the headers and the GOODS v2.0 mosaic, which we corrected for by introducing a 0°.3 relative rotation. The total exposure time in each filter per pointing was 5218 s, and the six pointings were reduced separately and all registered to the GOODS v2.0 ACS mosaics rebinned by 2×2 pixels. Each pointing surveyed a region of 3.3 arcmin^2 to maximum depth (i.e. where all six exposures overlapped), with the edge regions covered by fewer exposures. In this analysis, we only consider the deepest region of uniform depth, covering a total of 20 arcmin^2 over the six pointings.

The final frames had units of electrons/second, and we take the standard ACS zero-points for the UDF images. For WFC3, we use the recent zero-points reported on http://www.stsci.edu/hst/wfc3/phot_zp_lbn, where the F098M Y band has an *AB* magnitude zero-point of 25.68 (such that a source of this brightness would have a count rate of $1\,\mathrm{e^- \, s^{-1}}$), and the F125W J-band zero-point is 26.25. We note that the information in the image headers is slightly different by 0.1–0.15 mag, with zero-points of $Y_{ZP} = 25.58$ and $J_{ZP} = 26.10$.

2.1 Construction of catalogues

Candidate selection for all objects in the field was performed using version 2.5.0 of the SEXTRACTOR photometry package (Bertin & Arnouts 1996). For the z-drops, as we are searching specifically for objects which are only securely detected in the WFC3 Y band, with minimal flux in the ACS images, fixed circular apertures 0.6 arcsec in diameter were 'trained' in the Y image and the identified apertures used to measure the flux at the same spatial location in the z'-band image by running SEXTRACTOR in dual-image mode. This was repeated for all other ACS and WFC3 filters. For object identification, we adopted a limit of at least five contiguous pixels above a threshold of 2σ per pixel (on the data drizzled to a scale of 0.06 arcsec pixel^{-1}). This cut enabled us to detect all significant sources and a number of spurious detections close to the noise limit, or due to diffraction spikes of stars. As high-redshift galaxies in the rest-UV are known to be compact (e.g. Bremer et al. 2004; Bunker et al. 2004; Ferguson et al. 2004), we corrected the aperture magnitudes to approximate total magnitudes with the aperture correction appropriate for that filter; the aperture corrections were 0.23 mag in

Figure 1. Transmission curves for the ACS z'_{f850lp} and WFC3 Y_{f098m} and J_{f125w} filters. Also shown is the curve for the Y_{f105w} filter recently employed in studies of the HUDF.

Y band and 0.25 mag in *J* band, with the ACS bands having aperture corrections of ≈0.1 mag.

The 'MULTIDRIZZLE' procedure resamples and interpolates pixels, resulting in noise which is highly correlated. Rather than using the standard deviation of counts in the drizzled images to determine the noise level, we instead look at the individual reduced exposures (after flat-fielding and background subtraction), and a combination using integer-pixel shifts which preserves the noise characteristics. The noise in an individual *Y*-band exposure is $0.026\,e^-\,s^{-1}$, and in a combined pointing it is $0.011\,e^-\,s^{-1}$. We impose a brightness cut of $Y_{AB} < 27.0$ (after applying the aperture correction) corresponding to a $>6\sigma$ detection. Working at this secure signal-to-noise ratio ensures purity of the sample and robustness of the broad-band colours. Our limiting magnitude of $Y_{AB} = 27.0$ is equivalent to a star formation rate (SFR) of $4.5\,M_\odot\,yr^{-1}$ at $z = 7$, using the conversion from UV continuum luminosity of Madau, Pozzetti & Dickinson (1998) and assuming a Salpeter (1955) initial mass function and no correction for dust attenuation.

3 ANALYSIS

3.1 Candidate selection

Identification of candidates is achieved using the Lyman-break technique (e.g. Steidel et al. 1996), where a large colour decrement is observed between filters either side of Lyman α in the rest-frame of the galaxy. The flux decrement comes principally from the large integrated optical depth of the intervening absorbers (the Lyman α forest).

In Fig. 2, we illustrate how a colour cut of $(z - Y) > 0.8$ is effective at selecting sources at $z > 6.5$. The principal caveat is that for $(z - Y) < 1.7$ we may include contamination from low-mass galactic T and L dwarf stars and for $(z - Y) < 1.0$ from evolved systems at $z \approx 1.5$ where we pick up the Balmer/4000 Å break.

These interlopers can be discriminated against using additional colour information, and we use the *J*-band (F125W) images from
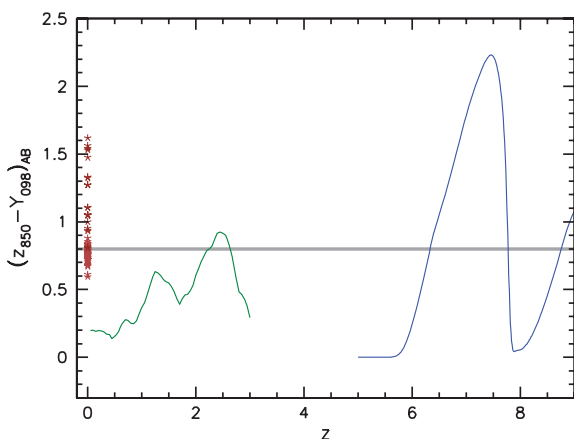
Figure 2. The evolution of the $(z' - Y)$ colour of starbursting galaxies, an instantaneous burst at $z = 10$ and low-mass L and T dwarf stars. The right-hand curve shows the colour evolution of a galaxy with UV spectral slopes of $\beta = -2.0$ (where $f_\lambda = \lambda^\beta$) damped below Lyman α by a factor of 100. The left-hand curve shows the colour evolution of an evolving stellar population that formed instantaneously at $z = 10$, and the red stars denote the observed colours of L and T dwarf stars (Golimowski et al. 2004; Knapp et al. 2004; Chiu et al. 2006). The grey horizontal line denotes our $(z' - Y)_{AB} = 0.8$ colour selection criteria.
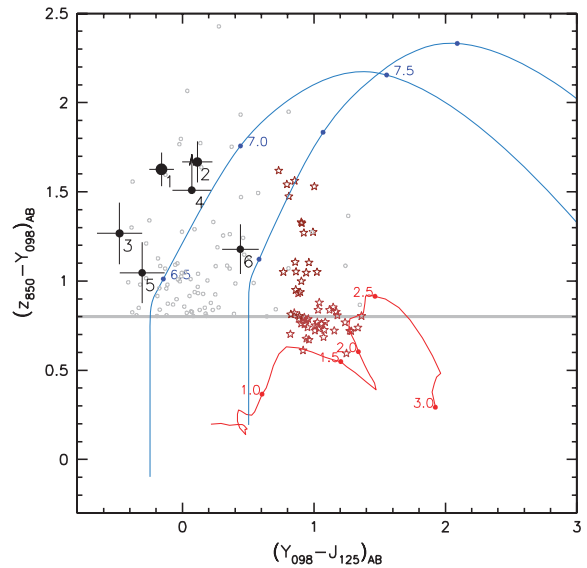

Figure 3. $(z' - Y)$ versus $(Y - J)$ colour–colour diagram illustrating the differentiation of high-redshift star-forming galaxies, low-mass L and T dwarf stars and lower redshift galaxies. The upper two curves show the colour evolution of model starbursting galaxies with UV spectral slopes of $\beta = -3$ (left) and $\beta = 0.0$ (right) (where $f_\lambda = \lambda^\beta$) damped below Lyman α by a factor of 100. The lower curve shows the colour evolution of an evolving stellar population that formed instantaneously at $z = 10$. Stars denote the observed colours of L and T dwarf stars (Golimowski et al. 2004; Knapp et al. 2004; Chiu et al. 2006). Objects matching our $z - Y > 0.8$ selection criteria and which are also undetected in the *BVi* imaging are denoted by the filled black circles and their 1σ errors (or lower limits). Objects which meet the $z - Y$ criteria but are detected in one or more of the *BVi* images are denoted by grey circles.

this *HST*/WFC 3 programme together with existing ACS *BVi*-band imaging to achieve this.

Galactic L and T dwarf stars can be distinguished from high-*z* sources by their position in $(z - Y)$–$(Y - J)$ colour plane (see Fig. 3), as the low-mass stars typically possess redder $(Y - J)$ colours than the high-*z* Lyman-break galaxies. Lower redshift objects with strong Balmer breaks can however be more difficult to distinguish. Galaxies with strong Balmer breaks at $z \approx 1.5$ can mimic the $z - Y$ colours of *z'*-drop galaxies. These Balmer break galaxies have dominant post-starburst populations, of age $\geq 100\,$Myr. They will potentially be undetected at shorter wavelengths (the ACS filters) if they do not have significant ongoing star formation (i.e. the rest-UV is faint). Such objects will, however, have quite red $Y - J$ colours (above the Balmer break) and hence will lie in a different position in $(z - Y)$–$(Y - J)$ colour space than the Lyman-break galaxies at $z \approx 7$ (see Fig. 3). Fig. 4(b) shows the photometry of an object in our sample which is well fitted by a Balmer break spectrum at $z = 1.3$ produced by an instantaneous burst of age 3000 Myr.
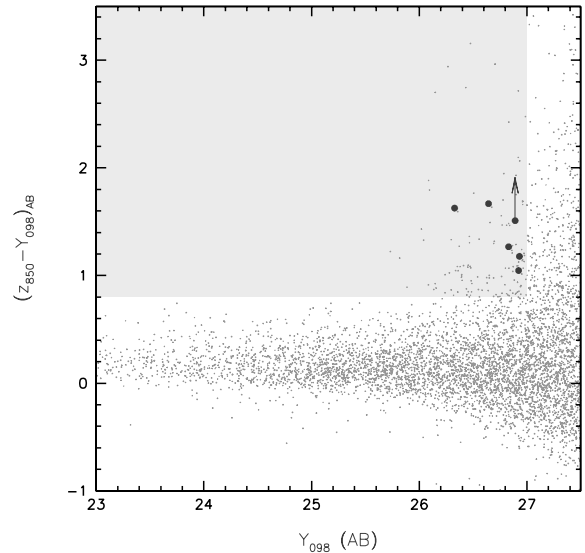
However, Balmer break galaxies can have bluer $Y - J$ colours if they have a more complicated star formation history, with a more recent or ongoing episode of star formation involving a small fraction of the stellar mass. At $z \approx 1.5$, these galaxies can lie in approximately the same position as $z \approx 7$ galaxies in the $(z - Y)$–$(Y - J)$ colour plane. Such objects will, however, also have a steep blue spectral slope shortwards of break, and will potentially be detectable at shorter wavelengths (with a $V - Y$ colour of ~1 at $z \approx 1.5$). At our catalogue limit of $Y_{AB} = 27.0$, these 'blue Balmer break' galaxies will have *V*-band detections in the ACS images of
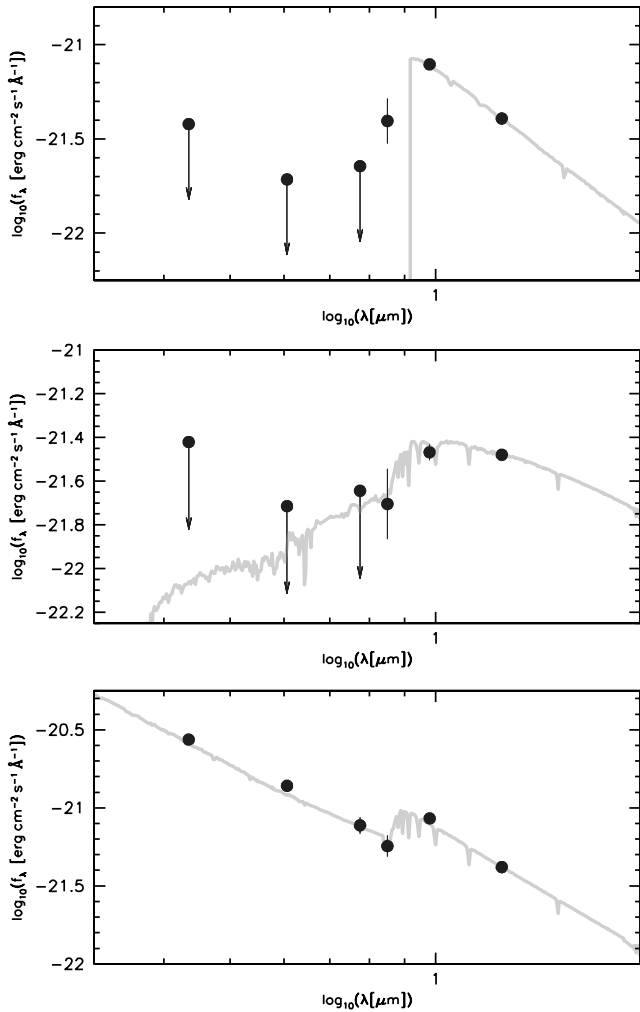
Figure 4. Example spectral energy distributions (SEDs) of objects meeting our $z - Y > 0.8$ selection criteria. Top (a): a candidate z-drop galaxy (points) and the synthetic SED of a $z \approx 7$ galaxy (line). Middle (b): photometry of a possible Balmer break galaxy and the synthetic spectra of a galaxy composed of a single 3000 Myr population at $z = 1.3$. Bottom (c): an object detected in the ACS BVi bands but which has a $J - Y$ colour consistent with high-z galaxies. The grey line denotes the synthetic SED of galaxy comprised of two populations: a 200 Myr old instantaneous burst and a 10 Myr old burst.

Figure 5. The $(z' - Y)$ colours of all objects in our catalogue (dots) as a function of Y-band magnitude. The grey shaded area denotes our Y_{AB}-band magnitude and $(z' - Y)_{AB}$ colour criteria. Objects meeting our full [undetected in the ACS B, V, i' imaging and consistent $(Y - J)_{AB}$ colour] selection criteria are marked by the larger circles.

GOODS-South. Both a synthetic and observed example of such an object is shown in Fig. 4(c).

Our initial selection of objects brighter than $Y_{AB} = 27.0$ and redder than $(z - Y)_{AB} = 0.8$ yielded 148 objects (shown in Fig. 5). Of these 37 per cent (55) are clearly spurious (e.g. diffraction spikes). Of the remaining 93 candidates all but six (6.5 per cent) have detections in the bluer B, V or i ACS bands at $>2\sigma$ (i.e. $B < 29.14$, $V < 29.16$, $i < 28.45$). Of the 93 non-spurious objects, a further eight (9 per cent) are detected in the ACS i band but are undetected at $>2\sigma$ in the B and V bands. These objects are possibly $z \approx 6$ i-drop galaxies rather than $z \approx 7$ (indeed we recover galaxies CDFS-2290242079 and CDFS-2226643007 from the ACS GOODS i-drop catalogue of Bouwens et al. 2006). Adopting a conservative approach, we do not include these i-band-detected sources in our final sample. Photometry of our six remaining z-drop candidates are presented in Table 1, and the ACS and WFC 3 images are shown in Fig. 6.

We also consider the available deep Multiband Imaging Photometer for *Spitzer* (MIPS) 24 μm imaging of the field which covers all of our survey area. This MIPS band is sensitive to thermal re-emission from dust in moderate redshift sources (powered either by highly obscured star formation or AGN activity), but we would not expect strong emission from $z \sim 7$ sources (rest-frame 3 μm). None of our six candidates are clearly detected (with < 10 μJy at 2σ); however, objects 2, 3 and 6 are confused by nearby sources. These objects nevertheless appear undetected, further supporting the assertion that our candidates are of high-redshift origin.

There is a 5-year interval between the ACS images and the WFC3 observations, which means that another possible source of contamination are transient objects (e.g. supernovæ), which might have brightened since the ACS data were taken. Indeed, the recent WFC3 images of the HUDF reveal a probable supernova when compared with the deep ACS imaging in 2004 (Bunker et al. 2009; Oesch et al. 2009; Yan et al. 2009). The WFC 3 Y-band filter (F098M) used in the wide-field GOODS-South imaging presented here has greater overlap in wavelength with the z band compared with the WFC 3 F105W filter used for the HUDF, which means that there is likely to be flux in the z band for most $z \approx 7$ candidates. Indeed, in all but one case, however, each of the candidates are also detected (faintly) in the ACS z-band images, implying they are not extreme transient objects such as supernovae. The one object (candidate 4) which is undetected in the z-band images has a 2σ lower limit of $(z - Y)_{AB} > 1.5$. This, combined with its $Y - J$ colour, suggests that it is still consistent with being a high-z star-forming galaxy (Fig. 3). Thus, we include this object in our final candidate list.

3.2 Number density of galaxies

Observations of Lyman-break galaxies at $z > 4$ have indicated significant evolution of the LF over cosmic time, in particular the discovery that the number density of luminous star-forming systems at $z \sim 6$ (the i-drops) is much less than in the well-studied U-drop

Table 1. z-band dropout candidate $z \approx 7$ galaxies meeting our selection criteria.

ID	RA Dec. J2000	z_{AB}	Y_{AB}	J_{AB}	$(z-Y)_{AB}$	$(Y-J)_{AB}$	SFR$_{z=7}$(M$_\odot$ yr^{-1})
1	03:32:15.997 −27:43:01.44	27.95 ± 0.44	26.32 ± 0.07	26.48 ± 0.05	1.62 ± 0.44	−0.16 ± 0.09	8.6
2	03:32:25.285 −27:43:24.25	28.31 ± 0.56	26.64 ± 0.09	26.53 ± 0.06	1.66 ± 0.57	0.11 ± 0.11	6.3
3	03:32:29.693 −27:40:49.88	28.09 ± 0.47	26.82 ± 0.11	27.30 ± 0.12	1.26 ± 0.48	−0.48 ± 0.17	5.3
4	03:32:29.541 −27:42:04.49	>28.4 (2σ)	26.89 ± 0.12	26.82 ± 0.08	>1.51 (2σ)	0.07 ± 0.14	5.0
5	03:32:37.833 −27:43:36.55	27.96 ± 0.41	26.92 ± 0.12	27.22 ± 0.11	1.04 ± 0.43	−0.30 ± 0.17	4.8
6	03:32:24.094 −27:42:13.85	28.10 ± 0.47	26.93 ± 0.12	26.49 ± 0.05	1.17 ± 0.49	0.44 ± 0.13	4.8

Note. The SFR has been derived using the conversion from UV luminosity density from Madau, Pozzetti & Dickinson (1998) and assuming the galaxies lie at $z = 7.0$.
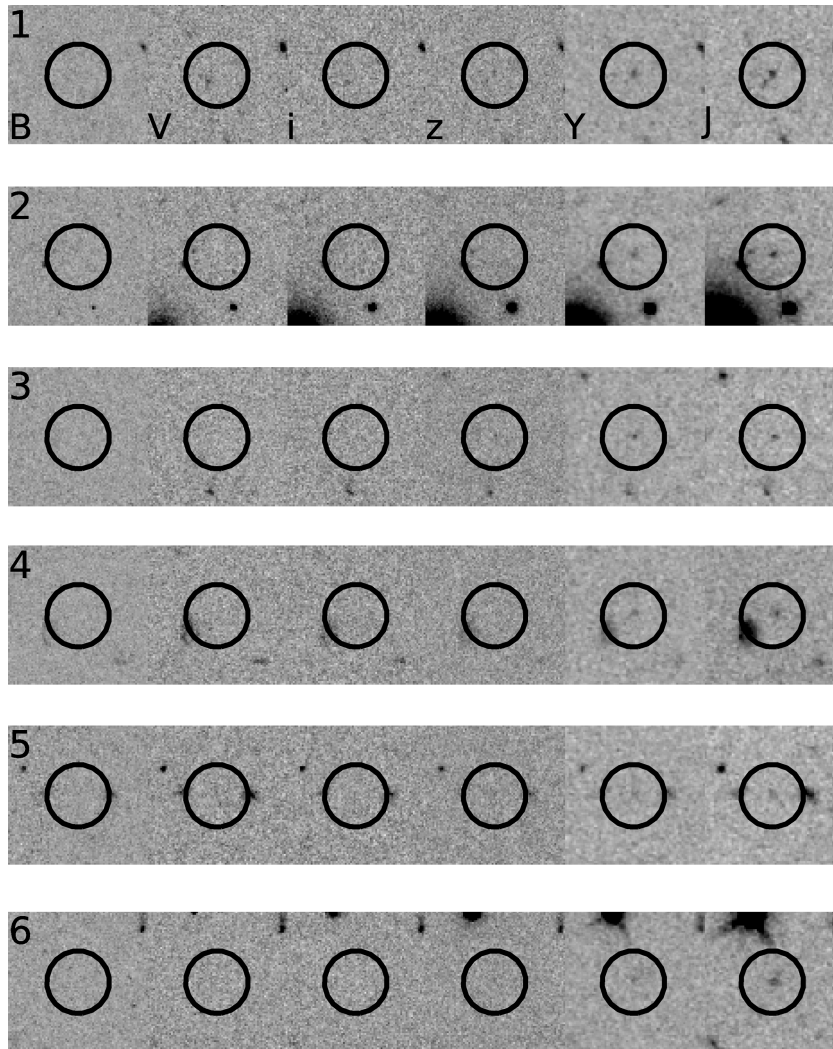
Figure 6. Postage stamp images of our candidates. ACS B, V, i, z images are shown alongside the WFC3 Y and J bands for each of our candidates. Each image is 2.4 arcsec across, with north up and east to the left.

and B-drop population at $z \approx 3$–4 (e.g. Lehnert & Bremer 2003; Stanway et al. 2003; Bunker et al. 2004; Bouwens et al. 2004, 2006).

Recent results from the z-drops indicate that this trend continues to $z = 7$–9 (Bouwens et al. 2009; Bunker et al. 2009; Oesch et al. 2009; Ouchi et al. 2009; Hickey et al. 2010; McLure et al. 2010). The new WFC3 data over several pointings allow us to constrain the LF around $Y_{AB} = 26$–27, a key region around $L^*_{\mathrm{UV}\,z\sim6}$ with too small numbers in the single HUDF pointing (only one object along with a

probable supernova contaminant) but too faint to be explored in the ground-based Y-band surveys. We also note that the F098M filter used in the data presented here does not go as red as the F105W WFC 3 filter used to survey the HUDF (see Fig. 1), so we are biased towards slightly lower redshifts than $z = 7$.

We have six candidates brighter than $Y_{AB} = 27.0$ which are undetected in the ACS B, V, i bands and with $(z - Y)_{AB} > 0.8$. We survey 20 arcmin^2 over the six pointings (where we consider only

Table 2. Observed and predicted surface densities of *z*-drop assuming different colour selections and LFs.

Colour cut	Limiting magnitude	Observed	$z = 3$ pred.[a]	$z = 6$ pred.[b]	$z = 7$ pred.[c]
0.8	26.5	0.051 ± 0.051	0.926	0.241	0.038
0.8	27.0	0.303 ± 0.123	2.114	0.722	0.147
1.0	26.5	0.051 ± 0.051	0.712	0.173	0.026
1.0	27.0	0.303 ± 0.123	1.678	0.546	0.106
1.3	26.5	0.051 ± 0.051	0.388	0.079	0.010
1.3	27.0	0.152 ± 0.087	0.987	0.284	0.049

[a]Assuming the Reddy et al. (2009) $z = 3$ UV LF.
[b]Assuming the Bouwens et al. (2006) $z = 6$ UV LF.
[c]Assuming the Bouwens et al. (2008) $z = 7$ UV LF.
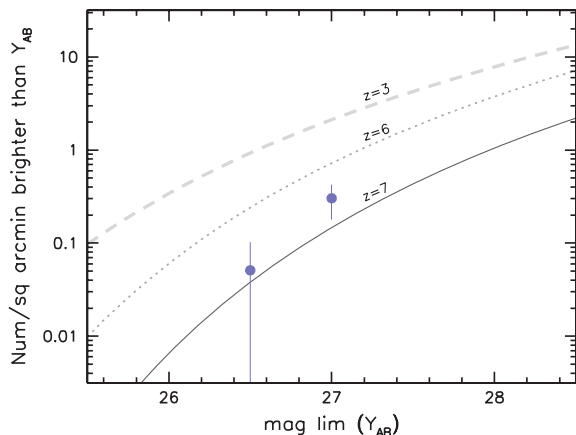
Figure 7. The cumulative surface density of *z*-drop galaxies (*y*-axis) brighter than a limiting magnitude Y_{lim} (*x*-axis). Our new results from the WFC 3 imaging of the GOODS–South field with the F098M filter are shown as the points. The dashed curve is the prediction using the UV LF derived for the $z = 3$ Lyman-break galaxies by Reddy et al. (2009), the dotted curve is the LF at $z = 6$ from Bouwens et al. (2006) and the solid line is the suggested $z = 7$ LF from Bouwens et al. (2008).

the deepest region where all six individual exposures per pointing overlap). Our surface densities are presented in Table 2 and Fig. 7, where the error comes from the Poisson statistics.

We now compare our observed surface density of $z \approx 7$ *z*-drop candidates with that expected from a range of LFs derived for Lyman-break galaxies at lower redshifts. We use the filter response curves to assess which redshifts will satisfy our colour cut, assuming a simple model spectrum for this high-redshift star-forming galaxy obeying a power law $f_\lambda \propto \lambda^\beta$ above Lyman α with a 99 per cent flux decrement below due to the Lyman α forest during the Gunn–Peterson era (and no flux below the 912 Å Lyman limit). For the UV spectral slope, we adopt a value of $\beta = -2$ consistent with the values reported for high-redshift galaxies (Stanway, McMahon & Bunker 2005), although we stress the number of objects is not particularly sensitive to small variations in β.

To compare our observations with predictions, we consider three UV LFs and note that for our assumed $\beta = -2.0$ (flat in f_ν) there is no *k*-correction necessary to the *AB* magnitudes between the various determinations of the UV continuum at 1300–1700 Å . To assess evolution to $z \approx 3$, we use the recent Reddy & Steidel (2009) determination of the Schechter LF, which has a steep faint end slope of $\alpha = 1.73$ and characteristic luminosity of $M_{UV}^* = -20.97$ and number density of $\phi^* = 0.00171 \, \text{Mpc}^{-3}$. For our comparison to galaxies at $z \approx 6$, we adopt the Bouwens et al. (2006) determination

which has a similar faint end slope and $\phi^* = 0.00206 \, \text{Mpc}^{-3} \, M_{UV}^* = -20.25$. Finally, we consider the proposed $z \sim 7$ LF of Bouwens et al. (2008) with $\phi^* = 0.0011 \, \text{Mpc}^{-3}$, $M_{UV}^* = -19.8$ and a similar α. Our observations and predictions of the number densities of galaxies are summarized in Table 2 for a range of colour cuts $(z' - Y) \in \{0.8, 1.0, 1.3\}$. Our observations suggest dramatic evolution between $z \approx 6$ and ≈ 7, with the observed number of *z*-drops 4σ below the no-evolution prediction. Our number density at $Y_{AB} < 27$ is consistent with that obtained from our recent analysis (Bunker et al. 2009) of the UDF (0.24 ± 0.24 arcmin^2). However, it is roughly twice that suggested by the $z \approx 7$ LF of Bouwens et al. (2008), although we emphasize that our statistical error is ≈ 40 per cent, and we estimate that the cosmic variance over our new data set will contribute a 30–40 per cent uncertainty (Trenti & Stiavelli 2008). This is a significant improvement upon the 4.2 arcmin^2 HUDF which contained only a single galaxy brighter than $Y = 27$ (e.g. Bunker et al. 2009), precluding a reliable measure of the normalization of the LF owing to the large Poisson error (~ 100 per cent) and cosmic variance (~ 50 per cent) for sources in this magnitude range.

The numbers of z'-drops discovered in this paper in the GOODS–South ERS–WFC3 observations are consistent with the deeper but smaller area HUDF (Bunker et al. 2009 and Fig. 7), accounting for differences in the shape of the *Y*-band filter bandpass. We consider the implications for reionization in Bunker et al. (2009): for our observed surface densities of z'-drops, the integrated SFR density [integrated down to $M_{UV} = -19.35$ (*AB*), equivalent to 0.1 L_{UV}^* at $z \approx 3$] is insufficient to achieve reionization unless the faint end slope is very steep ($\alpha \sim < -1.9$) and the escape fraction implausibly high ($f_{esc} > 0.5$). However, the number of ionizing photons is determined by the UV spectral slope (which is sensitive to the initial mass function, dust extinction, metallicity and star formation history). There are strong indications that the spectral slopes of our $z \approx 7$ Lyman-break galaxies are bluer than at lower redshift, and this evolution might make up the shortfall in ionizing photons.

The six *z*-drop galaxies presented here have SFRs of 5–10 $M_\odot$ yr^{-1}, assuming they are at $z = 7$. For a rest-frame equivalent width of 10 Å for Lyman α (typical of Lyman-break galaxies at modest redshift, $z \approx 3$–4, Steidel et al. 1999) this would correspond to a line flux of 1–2×10^{-18} erg cm^2 s^{-1}, and for larger equivalent widths of 30 Å which may be more typical of the $z > 5$ population (Stanway et al. 2004b; Vanzella et al. 2009) these galaxies may exhibit Lyman α line emission fluxes 3–6×10^{-18} erg cm^2 s^{-1}. These fluxes are within the capability of red-sensitive optical spectrographs on 8–10 m telescopes with long integrations. Given the large fraction of $z = 5$–6 dropouts in the same luminosity range that show such strong Lyman α emission (Stark et al., in preparation),

this sample should enable us to test whether the prevalence of Lyman α emitters declines over $6 < z < 7$, as expected given observations of narrow-band-selected Lyman α emitters (e.g. Ota et al. 2008).

4 CONCLUSIONS

In this work, we have searched for star-forming galaxies at $z \approx 7$ utilizing the Lyman-break technique on newly acquired F098M Y-band images from WFC3 on the *HST*. Through the comparison of these images to existing Hubble ACS F850LP z-band images, we identified objects with red colours, $(z - Y) > 0.8$, indicative of a break in the spectrum. We explore an area five times larger than the recent WFC 3 imaging of the HUDF. The new wider field data in GOODS-South probe down to $Y_{AB} = 27$, equivalent to $\approx L^*_{UV}$ at $z = 7$.

Using additional imaging (ACS B, B, i bands from GOODS v2.0, and WFC3 F125W J band) we removed contaminating objects which were either detected in the bluer ACS bands or with observed near-IR colours inconsistent with high-redshift star-forming galaxies.

This selection criteria left six candidates down to a limiting magnitude $Y_{AB} < 27.0$ (equivalent to a SFR of $4.5\,\mathrm{M_\odot\,yr^{-1}}$ at $z = 7$) of which all but one were detected in the z band (and are thus likely not to be transients). This implies a surface density of objects brighter than $Y_{AB} = 27.0$ of $0.30 \pm 0.12\,\mathrm{arcmin^2}$; a value smaller than both the predictions based on the observed $z \approx 3$ and ≈ 6 LFs, suggesting continued evolution of the LF beyond $z = 6$.

Knowledge of the surface density of dropouts in this magnitude range is crucial in constraining the LF, as current estimates of the $z \approx 7$ LF indicate that an L_* galaxy has a magnitude of $Y \sim 27$ (e.g. Bouwens et al. 2008). Determining the UV LF is crucial in order to address whether star-forming galaxies could plausibly have provided the Lyman continuum photons necessary to re-ionize the Universe .

Given the difficulty that ground-based surveys face in probing faintwards of $Y = 26$, larger-area surveys with *HST*/WFC3 ($\sim$100 arcmin^2) probing to similar depths $[Y(6\sigma) \sim 27.2]$ as the data set presented in this paper will deliver a factor of 2 improvement in the Poisson uncertainty and a significant decrease in the uncertainty due to cosmic variance.

ACKNOWLEDGMENTS

REFERENCES

Bertin E., Arnouts S., 1996, A&AS, 117, 393
Bouwens R. J. et al., 2004, ApJ, 616, L79
Bouwens R. J. Illingworth G. D., Blakeslee J. P., Franx M., 2006, ApJ, 653, 53
Bouwens R. J., Illingworth G. D., Franx M., Ford H., 2008, ApJ, 686, 230
Bouwens R. J. et al., 2009, ApJ, submitted (arXiv:0909.1803)
Bremer M. N., Lehnert M. D., Waddington I., Hardcastle M. J., Boyce P. J., Phillipps S., 2004, MNRAS, 347, L7
Bunker A. J., Stanway E. R., Ellis R. S., McMahon R. G., McCarthy P. J., 2003, MNRAS, 342, L47
Bunker A. J., Stanway E. R., Ellis R. S., McMahon R. G., 2004, MNRAS, 355, 374
Bunker A. et al., 2009, MNRAS, submitted (arXiv:0909.2255)
Castellano M. et al., 2009, A&A, in press (arXiv:0909.2853)
Chiu K., Fan X., Leggett S. K., Golimowski D. A., Zheng W., Geballe T. R., Schneider D. P., Brinkmann J., 2006, AJ, 131, 2722
Dickinson M. et al., 2004, ApJ, 600, L99
Dow-Hygelund C. C. et al., 2007, ApJ, 660, 47
Ferguson H, C. et al., 2004, ApJ, 600, 107
Giavalisco M. et al., 2004, ApJ, 600, L103
Golimowski D. A. et al., 2004, AJ, 128, 1733
Hickey S., Bunker A. J., Jarvis M., Chiu K., Bonfield D., 2010, MNRAS, in press (doi:10.1111/j.1365-2966.2009.15767.x) (arXiv:0909.4205)
Koekemoer A. M., Fruchter A. S., Hook R. N., Hack W., 2002, in Arribas S., Koekemoer, Whitmore B., eds, Proc. HST Calibration Workshop, Hubble after the Installation of the ACS and the NICMOS Cooling System. Space Telescope Science Institute, Baltimore, MD, p. 337
Knapp G. R. et al., 2004, AJ, 127, 3553
Lehnert M. D., Bremer M., 2003, ApJ, 593, 630
McLure R. J., Dunlop J. S., Cirasuolo M., Koekemoer A. M., Sabbi E., Stark D. P., Targett T. A., Ellis R. S., 2010, MNRAS, in press (doi:10.1111/j.1365-2966.2009.16176.x) (arXiv:0909.2437)
Madau P., Pozzetti L., Dickinson M., 1998, ApJ, 498, 106
Oesch P. A. et al., 2009, ApJL, in press (arXiv:0909.1806)
Oke J. B., Gunn J. E., 1983, ApJ, 266, 713
Ouchi M. et al., 2008, ApJS, 176, 301
Ouchi M. et al., 2009, ApJ, 706, 1136
Ota K. et al., 2008, ApJ, 677, 12
Reddy N. A., Steidel C. C., 2009, ApJ, 692, 778
Salpeter E. E., 1955, ApJ, 121, 161
Salvaterra R. et al., 2009, Nat, 461, 1258
Stanway E. R., Bunker A. J., McMahon R. G., 2003, MNRAS, 342, 439
Stanway E. R. et al., 2004a, ApJ, 604, L13
Stanway E. R., Bunker A. J., McMahon R. G., Ellis R. S., Treu T., McCarthy P. J., 2004b, ApJ, 607, 704
Stanway E. R., McMahon R. G., Bunker A. J., 2005, MNRAS, 359, 1184
Steidel C. C., Giavalisco M., Pettini M., Dickinson M., Adelberger K. L., 1996, ApJ, 462, 17
Steidel C., Adelberger K., Giavalisco M., Dickinson M., Pettini M., 1999, ApJ, 519, 1
Tanvir N. R. et al., 2009, Nat, 461, 1254
Trenti M., Stiavelli M., 2008, ApJ, 676, 767
Vanzella E. et al., 2009, ApJ, 695, 1163
Yan H., Windhorst R., Hathi N., Cohen S., Ryan R., O'Connell R., McCarthy P., 2009, ApJ, submitted (arXiv:0910.0077)

This paper has been typeset from a TEX/LATEX file prepared by the author.